

Probing Cosmology with Baryon Acoustic Oscillations using Gravitational Waves

SUMIT KUMAR^{1,2}

¹*Max-Planck-Institut für Gravitationsphysik (Albert-Einstein-Institut), D-30167 Hannover, Germany*

²*Leibniz Universität Hannover, D-30167 Hannover, Germany*

ABSTRACT

The third-generation (3G) gravitational wave (GW) detectors such as the Einstein telescope (ET) or Cosmic Explorer (CE) are expected to play an important role in cosmology. With the help of 3G detectors, we will be able to probe large-scale structure (LSS) features such as baryon acoustic oscillations (BAO), galaxy bias, etc. We explore the possibility to do precision cosmology, with the 3G GW detectors by measuring the angular BAO scale using localization volumes of compact binary merger events. Through simulations, we show that with a 3G detector network, by probing the angular BAO scale using purely GW observations, we can constrain the Hubble constant for the standard model of cosmology (Λ CDM) with 90% credible regions as $H_0 = 59.4^{+33.9}_{-17.7}$ km s⁻¹ Mpc⁻¹. When combined with BAO measurements from galaxy surveys, we show that it can be used to constrain various models of cosmology such as parametrized models for dark energy equations of state. We also show how cosmological constraints using BAO measurements from GW observations in the 3G era will complement the same from spectroscopic surveys.

Keywords: gravitational waves — cosmology — binary neutron stars — third generation detectors

1. INTRODUCTION

In the last few years, the detection of gravitational waves (GW) from the merger of compact objects has become a routine (Abbott et al. 2016, 2017a) and results in detailed catalogs of gravitational wave mergers (Abbott et al. 2021b; Nitz et al. 2021). The growth of the catalogs enabled us to probe various aspects of science, to list a few: i) inferring the population properties, such as the mass, spin and redshift distribution of the compact binaries (Abbott et al. 2021c), ii) testing the validity of general relativity (Abbott et al. 2021d), iii) constraining the equation of state and radii of neutron stars (Abbott et al. 2018a; Capano et al. 2020), iv) constraining the cosmic expansion history and inferring the value of the Hubble parameter (Abbott et al. 2021e), etc.

The idea of probing cosmology with GWs is not only exciting but also timely as there exists a tension between the value of the Hubble constant H_0 measured from low redshift data such as supernovae (SNe) (Riess et al. 2019) and the data from surveys from the

high redshift such as the cosmic microwave background (CMB) (Aghanim et al. 2020). For example, the value of H_0 as obtained from Planck 2018 results indicate $H_0 = 67.04 \pm 0.5$ km s⁻¹ Mpc⁻¹ (Aghanim et al. 2020), while the inferred value from the low redshift probes such as SNIa yields $H_0 = 74.03 \pm 1.42$ km s⁻¹ Mpc⁻¹ (Riess et al. 2019). A recent measurement of the local value of H_0 from the Hubble Space Telescope (HST) and SHOES team provides a constraint on the H_0 with ~ 1 km s⁻¹ Mpc⁻¹ uncertainty as $H_0 = 73.30 \pm 1.04$ km s⁻¹ Mpc⁻¹, which implies a 5σ difference with the value predicted by Planck 2018 measurements (Riess et al. 2021). All these measurements assume the standard model of cosmology known as the Λ CDM model.

The very first detection of GWs from the merger of a binary neutron star (BNS) (Abbott et al. 2017a) was accompanied by observations from various electromagnetic (EM) telescopes (Abbott et al. 2017b,c), which made it possible to put the very first constraints on the value of the Hubble constant from GW observations (Abbott et al. 2017d). Since then, binary black hole (BBH) merger events have also been used to put constraints on the Hubble parameter, by cross-correlating their localization volumes with the galaxy catalogs (Abbott et al. 2021a). The degeneracy between the mass and redshift of observed BBH mergers was also explored

along with the population models to put constraints on the value of H_0 (Mastrogiovanni et al. 2021). The recent estimates of the H_0 from recent GWTC-3 catalog with 68% CL indicates $H_0 = 68^{+8}_{-6} \text{ km s}^{-1} \text{ Mpc}^{-1}$ (Abbott et al. 2021e). Though the uncertainties on the value of H_0 measured from the GW observations is not at the level of resolving Hubble tension right now, we expect that in the near future, with more GW observations and improvements in the detector sensitivity, we can resolve this tension (Chen et al. 2021).

The current generation of detectors such as LIGO-Hanford, LIGO-Livingston (Aasi et al. 2015), Virgo (Acernese et al. 2015), and KAGRA (Akutsu et al. 2021) are set to undergo upgrades in various stages in upcoming years (Abbott et al. 2018b), and new detectors such as LIGO-India (Saleem et al. 2022) are expected to join the global detector network at some point in the future. Thanks to these network improvements, the source localization is expected to improve considerably (Fairhurst 2014). Furthermore, the proposed third-generation (3G) ground-based detectors such as Cosmic Explorer (CE) (Reitze et al. 2019; Evans et al. 2021) and the Einstein telescope (ET) (Sathyaprakash et al. 2012; Punturo et al. 2010) are expected to be operational sometime during the next decade. These detectors will be able to probe the Universe up to very high redshifts ($z \sim 10$) and will be able to detect thousands of GW merger events per year (Mills et al. 2018; Borhanian & Sathyaprakash 2022). Many of these GW mergers (at lower redshifts) are expected to be localized within a square degree so that the spatial distribution of the localization volumes of well-localized mergers can be used to probe the large-scale structure (LSS) of the Universe, *e.g.* by measuring the galaxy bias (Vijaykumar et al. 2020), or by detecting the baryon acoustic oscillations (BAO) peak (Kumar et al. 2022), solely from the GW observations. The evolution of the galaxy bias as a function of redshift can be used to do precision cosmology with GW merger events (Mukherjee et al. 2021).

In this work, we explore another aspect of probing cosmology with the 3G GW detectors through the LSS. We show that by detecting the angular BAO peak using localization volumes of mergers with the 3G GW detector network, we can put independent constraints on the value of H_0 . Moreover, by combining these results with the BAO measurements from the galaxy surveys, we should be able to put stringent constraints on various cosmological parameters for the standard model of cosmology, as well as on other phenomenological models for the dark energy parametrization. The BAO measurements from the spectroscopic surveys such as SDSS do not constrain the Hubble parameter H_0 on its own. In

order to put constraints on H_0 , the BAO measurements need to be combined with other observations such as SNIa, CMB data, etc (Alam et al. 2021). On the other hand, the BAO measurements, that will be obtained from the localization volumes of mergers of compact binary coalescence (CBC) sources with the 3G detector network, will have capabilities to constrain the Hubble parameter H_0 on its own. We show that by combining BAO observations from spectroscopic surveys and 3G GW observations, we will be able to put combined constraints on the cosmological model as both data sets are complementary to each other.

The structure of this paper is as follows. In section 2, we outline the existing methods to probe cosmology using the current and next generation of GW detectors. We also lay down the methodology to use the BAO measurements with GW merger events, to constrain cosmological models. In section 3, we use simulated data to apply these methods to constraint dark energy (DE) models. We use three parametrized DE models along with the standard Λ CDM model. In section 4, we summarize the results.

2. COSMOLOGY WITH GRAVITATIONAL WAVES

The data from various cosmological surveys indicate that at present, the major constituents of the Universe are dark energy, dark matter, and baryonic matter (Aghanim et al. 2020). One of the simplest models which describes the Universe is the so-called Λ CDM model, which interprets the dark energy component of the Universe in terms of the presence of a cosmological constant Λ term in the Einstein equations, along with cold dark matter (CDM), and the baryonic matter which represents all visible matter in the Universe (Riess & et al. 1998; Aghanim et al. 2020; Weinberg 2013).

The data from GW detectors consists of a time series $s(t)$ which contains noise $n(t)$ and might contain a GW signal $h(t)$. The GW signal from the merger of two compact objects is modelled as a function of the intrinsic parameters such as individual masses and spins, as well as extrinsic parameters such as the luminosity distance (D_L), the inclination angle of the binary with respect to the line of sight, the sky localization (right ascension and declination angles), etc. The localization volumes estimated for a GW event provide a posterior distribution on sky location (RA, dec) and D_L . If, somehow, we can estimate the redshift (z) of the GW event independently (Holz & Hughes 2005; Dalal et al. 2006; Nissanke et al. 2013), then using the $D_L - z$ relation from the so-called Hubble equation, we can put constraints on the parameters of the cosmological model, such as the Hubble parameter (H_0), the density parameter corresponding to

the matter component (Ω_{m0}), etc. The first detection of gravitational waves from the merger of binary neutron stars, known as GW170817 (Abbott et al. 2017a) provided one such opportunity. The electromagnetic (EM) afterglow of GW170817 was measured by various telescopes across the globe. It provided the constraints on H_0 using a GW event for the first time (Abbott et al. 2017d). Since then, various schemes have been used to probe cosmology by GW observations. For binary black holes (BBH) merger events, the localization posteriors can be cross-correlated with the galaxy catalogs to put constraints on H_0 (Abbott et al. 2021a). Other methods exploit the degeneracy between the inferred component masses from GW events and their redshift by putting combined constraints on H_0 and on the population parameters (Mastrogiovanni et al. 2021).

2.1. Baryon Acoustic Oscillations

BAO are imprints on the distribution of matter from the very early Universe. In the standard model of cosmology, the evolution of the Universe is described through three major phases where the dominant component is radiation, matter, and dark energy respectively. In the very early time, the Universe is assumed to have gone through a period of rapid accelerated expansion, known as inflation, resulting in an extremely homogeneous Universe (Guth 1981; Linde 1982; Baumann 2011). After this period, the Universe enters what is known as the radiation-dominated era, when the temperature of the Universe was very high, so that the protons and electrons could not form a stable hydrogen atom. The Universe was dominated by dark matter, and a hot plasma soup of electrons, protons, and photons. The small perturbations of Gaussian nature in the very early Universe acted as seeds for inhomogeneities and those perturbations grew with time. The competing forces between gravity and electromagnetic radiation pressure in the fluid generated the perturbations which act as sound waves in the hot plasma. About 380,000 years after the big bang, when the temperature of the Universe dropped to a level such that the electrons and protons could combine to form hydrogen atoms, the photons are set free, known as the cosmic microwave background (CMB), and the sound waves were frozen (Hu & Dodelson 2002; Aghanim et al. 2020). These features have been preserved in the distribution of matter as the Universe evolved. These imprints are called Baryon acoustic oscillations (BAO) (Bassett & Hlozek 2009; Weinberg et al. 2013) and can be seen in the two-point correlation function (2PCF) estimated from the distribution of galaxies (Peebles 1980; Landy & Szalay 1993; Eisenstein et al. 2005). The comoving sound

horizon or BAO scale: r_s corresponds to the distance sound waves traversed before they become frozen. The first confident detection of this BAO feature with 3.4σ certainty was reported by the Sloan Digital Sky Survey (SDSS) data release 3 (Eisenstein et al. 2005) by measuring 2PCF of the luminous red galaxies. The BAO scale r_s can be used to probe the cosmology as it provides a standard ruler.

2.2. Cosmology using the Large-Scale Structures of the Universe

The large-scale structures (LSS) ($> \mathcal{O}(10 \text{ Mpc})$) of the Universe can be studied by probing the distribution of matter, such as in the galaxy surveys, using the 2PCF $\xi(r)$, which is related to the excess probability δP with respect to the expected random distribution, of finding a pair of galaxies separated by a distance r ,

$$\delta P(r) = n[1 + \xi(r)]dV, \quad (1)$$

where n is the average number of galaxies per unit volume and dV is the infinitesimal volume or volume element around a galaxy. The 2PCF $\xi(r)$ can be estimated from the matter overdensity field $\delta(\mathbf{x}) := \rho(\mathbf{x})/\bar{\rho} - 1$, where $\rho(\mathbf{x})$ is the local matter density at position \mathbf{x} and $\bar{\rho}$ is the average matter density of the Universe, as

$$\xi(r) = \langle \delta(\mathbf{x})\delta(\mathbf{y}) \rangle, \quad (2)$$

where the operation $\langle \cdot \rangle$ represents the ensemble average over a large volume compared to the scales we are probing. An important assumption here is the statistical homogeneity and isotropy of the Universe. Due to these assumptions, the correlation function ξ depends only on the magnitude of the separation between points \mathbf{x} and \mathbf{y} , $r = |\mathbf{x} - \mathbf{y}|$. In general, $\xi(r)$ also evolves with the redshift, but if one restricts the analysis to a given redshift bin, the correlation function in that redshift bin can be assumed to be constant. Since the dark matter is more abundant than the baryonic matter (which constitutes the ‘visible’ galaxies, and intergalactic medium), the galaxies are expected to follow the gravitational potential well due to dark matter, and to a good approximation, at large scales, the 2PCF of galaxies $\xi_{gal}(r)$ will be related to the dark matter 2PCF $\xi_{DM}(r)$ via a factor b_{gal} called ‘galaxy bias’ as $\xi_{gal}(r) = b_{gal}^2 \xi_{DM}(r)$. In general, this bias, also known as ‘clustering bias’ can be scale- and redshift-dependent (Coles & Erdogdu 2007).

Apart from the galaxy bias, the 2PCF is also used to detect other LSS features, such as the BAO, from the distribution of matter. As r_s can be considered a standard ruler, detecting the BAO peak at different redshifts

Table 1. The list of parametrized dark energy models considered in this work. Ω_{m0} and Ω_{r0} are present day density parameters for matter and radiation component respectively. w, w_0 , and w_a are related to the dark energy parametrization. The parameter h is related to Hubble parameter H_0 as $h = \frac{H_0}{100 \text{ km s}^{-1} \text{ Mpc}^{-1}}$.

S.	No.	Model	Hubble Equation	parameters
	1.	Λ CDM	$h(z) = \sqrt{\Omega_{m0}(1+z)^3 + \Omega_{r0}(1+z)^4 + 1 - \Omega_{m0} - \Omega_{r0}}$	Ω_{m0}, h
	2.	w CDM	$h(z) = \sqrt{\Omega_{m0}(1+z)^3 + \Omega_{r0}(1+z)^4 + (1 - \Omega_{m0} - \Omega_{r0})(1+z)^{-3(1+w)}}$	Ω_{m0}, h, w
	3.	$w_0 w_a$ CDM	$h(z) = \sqrt{\Omega_{m0}(1+z)^3 + \Omega_{r0}(1+z)^4 + (1 - \Omega_{m0} - \Omega_{r0})(1+z)^{3(1+w_0+w_a)} \exp\left(-\frac{3w_a z}{1+z}\right)}$	Ω_{m0}, h, w_0, w_a

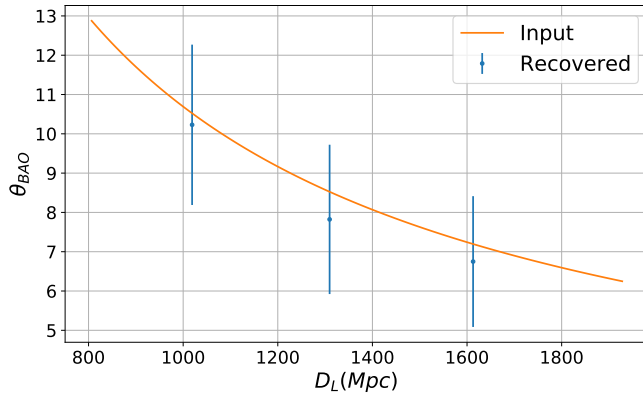


Figure 1. The recovery of the BAO angular scale θ_{BAO} with BNS merger events (for a 3G detector network) centered around different values of D_L in shells of about $\sim 150h^{-1}$ Mpc. The solid continuous curve represents the relation between θ_{BAO} and luminosity distance D_L to the shell for Λ CDM model used in simulations using parameters from the *Planck2018* results (Aghanim et al. 2020)

provides an independent method to probe the cosmological parameters. Instead of using the three-dimensional correlation function $\xi(r)$, one can also use the two-point angular correlation function (2PACF) $\omega(\theta)$ by considering the galaxies in different redshift bins and projecting them along the radial direction in the shell, keeping in mind that the chosen shell should be small enough for the linear power spectrum $P(k, z)$ to remain constant in the redshift bin, i.e., $P(k, z) \sim P(k)$ for $z \in [z - dz/2, z + dz/2]$. The BAO scale r_s is related to the angular scale θ_{BAO} and to the angular diameter distance D_A as,

$$\theta_{BAO}(z) = \frac{r_s}{(1+z)D_A(z)} \quad (3)$$

By estimating the angular BAO scale $\theta_{BAO}(z)$ at a given redshift z , one can use the above relation to put

constraints on the cosmological parameters which are embedded in the Hubble equation while calculating the angular diameter distance,

$$D_A(z; \Theta) = \frac{c}{H_0} \frac{1}{1+z} \int_0^z \frac{dz'}{h(z'; \Theta)} \quad (4)$$

where $h(z; \Theta)$ is the normalized Hubble equation with parameters Θ which depend on the cosmological model. For example, the normalized Hubble equation (at nearby redshifts) for the spatially flat Λ CDM model is,

$$h(z) = \sqrt{\Omega_{m0}(1+z)^3 + \Omega_{r0}(1+z)^4 + 1 - \Omega_{m0} - \Omega_{r0}}, \quad (5)$$

where $\Omega_{m0} = 3H_0^2 \rho_m / (8\pi G)$ is called the density parameter for matter (which includes dark matter as well as baryonic matter) at present ($z = 0$). Ω_{r0} is the density parameter corresponding to the radiation component. Ω_{d0} and Ω_{b0} represent density parameters corresponding to the dark matter and baryonic matter, respectively. It follows that $\Omega_{d0} + \Omega_{b0} = \Omega_{m0}$. Function $h(z)$ is called normalized Hubble parameter and is related to Hubble parameter $H(z)$ as $h(z) = \frac{H(z)}{H_0}$, where H_0 is the Hubble constant. In this study, we assume that the spatial curvature is zero, and we use the relation $\Omega_{m0} + \Omega_{r0} + \Omega_{\Lambda0} = 1$.

In the spectroscopic surveys, the BAO scale appears in the line-of-sight direction and the transverse direction. In the line of sight direction, the Hubble parameter $H(z)$ can be measured as $c\Delta z/r_s$ where Δz is the redshift range corresponding to the BAO scale. The corresponding Hubble distance at that redshift will be $D_H(z) = c/H(z)$. In the transverse direction, the BAO scale r_s is related to the comoving angular diameter scale $D_M(z)$ to the angular BAO scale θ_{BAO} as $r_s = D_M(z)\theta_{BAO}$. The spectroscopic surveys provide the measurements of $D_H(z)/r_s$ and $D_M(z)/r_s$. This can be combined into a single quantity describing spherical averaged distance

$D_V(z)/r_s$ where $D_V(z) \equiv [zD_M^2(z)D_H(z)]^{1/3}$ (Giostri et al. 2012; Alam et al. 2021)

2.3. Probing the Large Scale Structures with Gravitational Waves

As we expect the 3G detector network to provide a large number of well-localized GW merger events, the natural question arises: can we extend the similar methods as used for galaxies to probe the LSS with the distribution of GW observations using their localization volumes? Recent studies have shown that by cross-correlating localization volumes with galaxy catalogs, the LSS features such as the galaxy bias can be probed (Mukherjee et al. 2021). In this study, we are interested in probing the LSS purely with GW observations, without cross-correlation with galaxy catalogs.

The challenges in probing the LSS with just GW observations are twofold: i) the localization volumes obtained from the posteriors of GW events are currently very wide ($\mathcal{O}(10) - \mathcal{O}(100)$ Mpc for D_L and $\mathcal{O}(100) - \mathcal{O}(1000)$ square degrees for the sky localization) (Abbott et al. 2018; Petrov et al. 2022), which washes away most of the features in the LSS, and ii) the number of events which can be detected by current-generation GW detectors are not enough to probe the LSS. However, the planned 3G GW detectors such as the ET and CE are not only expected to have an order of magnitude better sensitivity compared to current detectors, but also expected to be more sensitive at low frequencies. This will allow the 3G detector network to detect enough events with precise enough localization volumes to make it possible to probe the LSS purely with GW events. It has been shown that with the 3G detector network, with 5-10 years of observation time, it will be possible to probe the galaxy bias solely from the GW events (Vijaykumar et al. 2020). Using the nearby BNS localization volumes ($z < 0.3$), the angular BAO scale θ_{BAO} can also be probed with the help of the 3G detector network (Kumar et al. 2022).

The detection of the angular BAO scale θ_{BAO} at different redshifts from the GW localization volumes can be used as another cosmological probe. The localization volumes of the GW mergers can be divided into shells of luminosity distance $D_L(z)$ and $\theta_{BAO}(D_L)$ can be recovered (Kumar et al. 2022). We can then use the measurement of the BAO scale r_s from other surveys, such as CMB surveys, and use relation 3 to put constraints on the cosmological parameters. This gives us an independent approach to constrain cosmological parameters using combined GW-CMB data.

3. SIMULATIONS AND RESULTS

We make use of the simulations done in Kumar et al. (2022), where we use publicly available code: lognormal-galaxies (Agrawal et al. 2017) to create galaxy catalogs with the given correlation function $\xi(r)$ containing the BAO peak. These mock galaxy catalogs represent a realization of the Universe arising from the underlying density perturbations. These galaxies act as the host to the GW merger events. We then create a catalog of the BNS merger population consistent with the estimated merger rates obtained from the LVK analysis (Abbott et al. 2021). We use the network of 3G detectors containing an Einstein telescope (Punturo et al. 2010) in Europe, and two cosmic explorer detectors (Reitze et al. 2019; Evans et al. 2021) located in the USA and Australia. In table 2, we show the detector configuration and location.

In this study, we restrict ourselves to the BNS sources between the redshift range ($0.2 \leq z \leq 0.3$) for the following reasons:

- The BNS merger rate is intrinsically higher ($10 \text{ Gpc}^{-3} \text{ yr}^{-1} - 1700 \text{ Gpc}^{-3} \text{ yr}^{-1}$) compared to BBH merger rates ($\sim 17 \text{ Gpc}^{-3} \text{ yr}^{-1} - 44 \text{ Gpc}^{-3} \text{ yr}^{-1}$ at fiducial redshift $z = 0.2$) (Abbott et al. 2021c).
- Through simulations, we find that in the redshift range ($0.2 \leq z \leq 0.3$) we will have thousands of BNS events per year which are localized within a degree square in the sky (Kumar et al. 2022).

Therefore, with 5 – 10 years of accumulated data with 3G network, we will have enough highly localized BNS events which will enable us to calculate 2PACF $w(\theta)$ using the localization volumes from the posterior samples of detected BNS sources in various luminosity distance shells. We also show that using 2PACF, we will be able to detect the angular BAO scale θ_{BAO} in different luminosity distance shells by fitting for the BAO peak (Kumar et al. 2022). We would like to emphasize that similar studies can be performed by other sources (like BBHs) if one can accumulate enough localized sources in a given D_L shell. Although, as we go further, the localization volumes of the sources become larger.

In figure 1, we show the recovery of the angular BAO scale at different shells centered around $D_L \sim 1010$ Mpc, 1310 Mpc, and 1620 Mpc. We use these mock measurements of angular BAO scale θ_{BAO} (from simulations) as the input data. The difference between the angular BAO scale measurement from GW sources and that from Galaxy sources is that the former is done in D_L space while later is done in redshift space. This makes the constraining power of the data sets complementary in terms of the set of parameters these data sets can constrain.

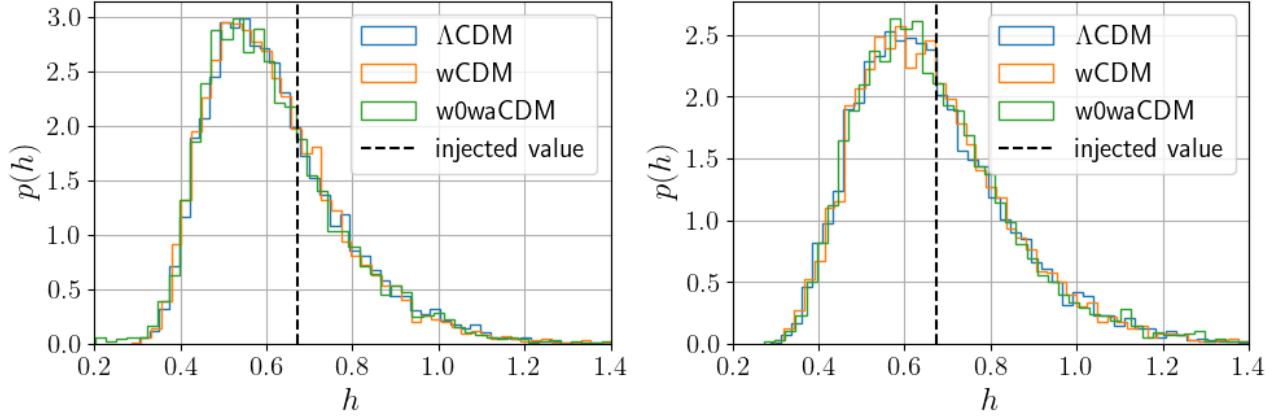


Figure 2. The 1D marginalized posterior distribution of the Hubble parameter $H_0 = 100h \text{ km s}^{-1} \text{ Mpc}^{-1}$ using the angular BAO scale measurements θ_{BAO} from simulated GW events with the 3G detector network in three shells centered at $D_L \sim 1000 \text{ Mpc}$, 1300 Mpc , and 1600 Mpc . The injected value is shown by the dashed vertical line. The three cosmological models used here are described in table 1. Left panel shows GW-BAO+CMB constraints and right panel shows constraints from GW-BAO+CMB+EM counterpart.

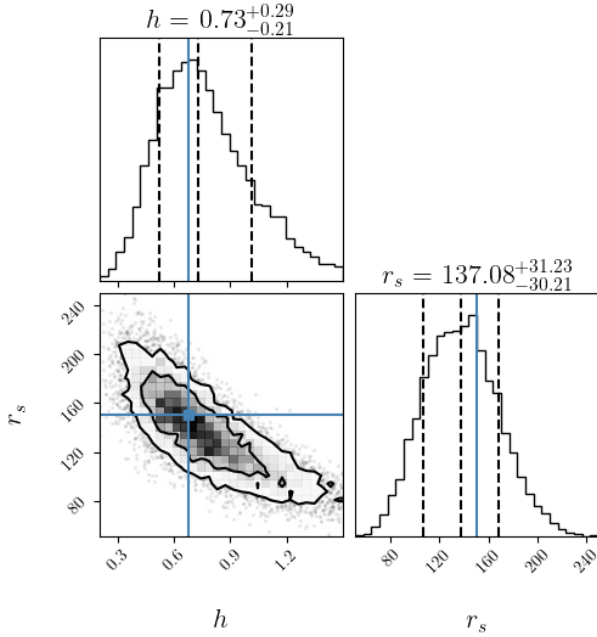


Figure 3. The GW-BAO+EM counterpart constraints on the Hubble parameter $H_0 = 100h \text{ km s}^{-1} \text{ Mpc}^{-1}$ and comoving BAO scale r_s [Mpc] for the ΛCDM model with BAO measurements from GW localization volumes (simulations). For the marginalized 1D posteriors, we show 68% bounds with the median value. For 2D contours, we show 60% and 90% regions. The injected values are shown by the blue lines.

In the Bayesian framework, the posterior probability distribution $p(\Theta|d, I)$ on the parameters Θ given the data d , and any prior information I is described as,

$$p(\Theta|d, I) = \frac{\mathcal{L}(d|\Theta, I)\pi(\Theta|I)}{p(d|I)}, \quad (6)$$

where $\mathcal{L}(d|\Theta, I)$ is the likelihood function which represents the probability of the data given the parameters Θ of the model. $\pi(\Theta|I)$ is the prior probability distribution on the parameters, and $p(d|I)$ is called the ‘Bayesian evidence’ or marginalized likelihood which acts as the normalization factor for the posterior distribution. We use the BAO measurements in different shells $\theta_{BAO}(D_L)$ as the data and define the likelihood function as,

$$\mathcal{L}(d|\Theta, I) \propto \exp\left(-\frac{1}{2} \sum_i \frac{(\theta_{BAO,i} - \theta_{BAO}(\Theta))^2}{\sigma_i^2}\right), \quad (7)$$

where Θ are the parameters describing the cosmological model. $\theta_{BAO,i}$ is the estimated angular BAO scale in the i -th shell corresponding to the effective luminosity distance D_L^i . σ_i is the error associated with the measurement of the BAO peak in i -th shell. The reason for assuming this form of likelihood function is that through simulations, we find that recovered values of θ_{BAO} from ~ 1000 catalogs we generated fits the Gaussian distribution around injected value. In general, the likelihood function 7 will also have correlation between the different shells and the full covariance matrix is needed to be calculated and incorporated. But, in this study, we assume the shells to be independent and do not expect that to change the conclusions of the study.

We use standard ΛCDM model as reference model in our simulations. Other phenomenological dark energy models as described in table 1 are also considered as recovery models, namely the $w\text{CDM}$ model and CPL parametrization $w_0w_a\text{CDM}$ model (Chevalier & Polarski 2001). We make use of the publicly available implementation of nested sampling based sampler DYNESTY (Speagle 2020) for parameter estimation.

Table 2. The 3G detector network configuration (location, noise curves, and low frequency cutoff f_{low}) used in the simulations done in Kumar et al. (2022). For the CE detector, subscript (2) represents (late) noise sensitivity curves and superscript (U, A) represents location of these detectors (USA, Australia). Similar detector configurations for CE and ET are taken in other studies such as in Nitz & Dal Canton (2021).

Abbreviation	Observatory	f_{low}	Noise Curve	Latitude	Longitude
C_2^U	Cosmic Explorer USA	5.2	CE2	40.8	-113.8
C_2^A	Cosmic Explorer Australia	5.2	CE2	-31.5	118.0
E	Einstein Telescope	2	ET-D Design	43.6	10.5

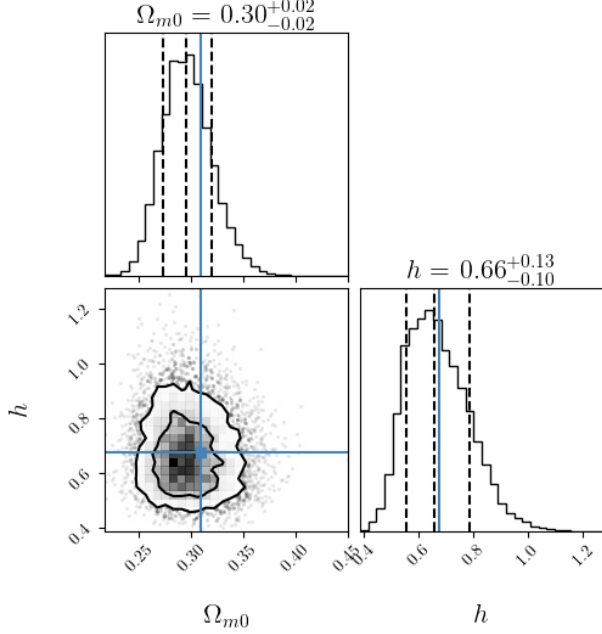


Figure 4. The combined constraints (GW-BAO+SDSS-BAO+CMB) on the Λ CDM model with BAO measurements from GW localization volumes (from simulations) and CMB/BAO constraints from the galaxy surveys. For the marginalized 1D posteriors, we show 68% bounds with the median value. For 2D contours, we show 60% and 90% regions. The injected values are shown by blue lines.

We use uniform prior on all the parameters in ranges $\Omega_{m0} \in [0.05, 1.0]$, $\Omega_{r0} \in [0.00001, 0.00015]$, $h \in [0.2, 1.5]$, $w, w_0 \in [-2, 0]$, and $w_a \in [-4, 4]$. In our simulations, the BAO measurements from GW observations are conducted in luminosity distance shells of thickness $150 h^{-1}$ Mpc and it is represented by the effective luminosity distance, D_L^{eff} , which is the midpoint of the D_L shell. We demonstrate further that $\theta_{\text{BAO}}(D_L^{\text{eff}})$ can be extracted at multiple D_L^{eff} (see figure 1). To fit the overall shape of the curve from the $\theta_{\text{BAO}} - z$ relation (equation 3), and account for the shell thickness, we treat the effective redshift of the shell, z_{eff} , as a free parameter corresponding to various D_L shells. The likelihood function 7 takes the

form:

$$\mathcal{L}(d|\Theta, I) \propto \exp\left(-\frac{1}{2} \sum_i \frac{(\theta_{\text{BAO},i} - \theta_{\text{BAO}}(z_{\text{eff}}^i, \Theta))^2}{\sigma_i^2}\right), \quad (8)$$

where $\theta_{\text{BAO},i}$ is the BAO angular scale measurement in i -th shell and

$$\theta_{\text{BAO}}(z_{\text{eff}}^i, \Theta) = \frac{r_s}{(1 + z_{\text{eff}}^i) D_A(z_{\text{eff}}^i, \Theta)}, \quad (9)$$

is the angular BAO scale corresponding to the luminosity distance shell, and Θ are the parameters of the cosmological model. We use the conditional uniform priors on z_{eff}^i such that it includes the luminosity distance shell for reasonable cosmology models: $z_{\text{eff}}^i \in [z(D_{L,i}^{\text{eff}} - 75, \Theta), z(D_{L,i}^{\text{eff}} + 75, \Theta)]$ for the three measurements of θ_{BAO} corresponding to the effective distance $D_L^{\text{eff}} \sim 1010$ Mpc, 1310 Mpc, and 1620 Mpc. For a chosen cosmology model, $z(D_L, \Theta)$ represents the redshift corresponding to the luminosity distance D_L and sampling parameters Θ . We use two strategies for parameter r_s :

1. Calculate r_s at given drag epoch z_d by estimating the distance travelled by sound waves in early universe for a cosmology model and parameters: Ω_{r0}, Ω_{m0} , and Ω_{b0} (Eisenstein & Hu 1998). Ω_{b0} is set it to Planck 2018 value (Aghanim et al. 2020). We call it GW-BAO+CMB constraints
2. We let the r_s vary as free parameter and use the uniform prior in range $r_s \in [50, 250]$ Mpc. We call it GW-BAO constraints.

Additionally, we investigate a particular scenario in which we may have an EM counterpart associated with one of the BNS signals. In such cases, we can obtain precise values for z_{eff} corresponding to the luminosity distance shell in which BNS with EM counterpart is detected. For this purpose, we use the luminosity distance shell corresponds to $D_L^{\text{eff}} \sim 1010$ Mpc from the simulation, and pivot it to fiducial observed redshift of $z_{\text{eff}} = 0.2$. For all other shells, we use the conditional

priors on z_{eff} as described above. These constraints are referred to GW-BAO+CMB+EM counterpart constraints.

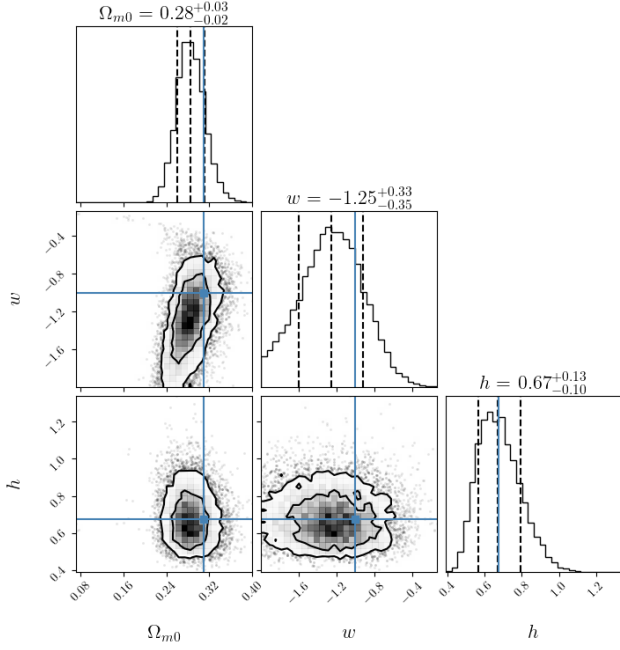


Figure 5. The combined constraints (GW-BAO+SDSS-BAO+CMB) on the w CDM model with BAO measurements from GW localization volumes (from simulations) and CMB/BAO constraints from the galaxy surveys. For the marginalized 1D posteriors, we show 68% bounds with the median value. For 2D contours, we show 60% and 90% regions. The injected values are shown by blue lines corresponding to the Λ CDM model with parameters consistent with the *Planck2018* results (Aghanim et al. 2020).

The Bayesian analysis with $\theta_{BAO}(D_L)$ measurements from the simulations provide constraints only on the Hubble parameter H_0 . Other cosmological parameters returns the uniform prior distribution indicating that data lacks the power to constrain these parameters. In figure 2, we show the recovery of the Hubble parameter for different cosmological models. It turns out that with GW-BAO+CMB data it is possible to constrain the Hubble parameter H_0 . The inferred value of H_0 (90% CL) for different models considered here are: i) Λ CDM model: $H_0 = 59.4^{+33.9}_{-17.7}$ km s⁻¹ Mpc⁻¹, ii) w CDM model: $H_0 = 59.0^{+32.2}_{-17.7}$ km s⁻¹ Mpc⁻¹, and iii) w_0w_a CDM model: $H_0 = 58.7^{+33.9}_{-17.7}$ km s⁻¹ Mpc⁻¹. For GW-BAO+CMB+EM constraints, the inferred H_0 values for different models turns out to be: i) Λ CDM model: $H_0 = 63.5^{+37.0}_{-21.3}$ km s⁻¹ Mpc⁻¹, ii) w CDM model: $H_0 = 63.9^{+35.6}_{-21.3}$ km s⁻¹ Mpc⁻¹, and iii) w_0w_a CDM model: $H_0 = 63.4^{+36.3}_{-20.6}$ km s⁻¹ Mpc⁻¹. The injected value for the H_0 is 67.04 km s⁻¹ Mpc⁻¹.

For GW-BAO + EM counterpart constraints, where r_s is treated as free parameter, the results are shown in figure 3. In this case, we are able to constrain two parameters: H_0 and r_s . As expected, the constraints on the H_0 are wider compared to the case where acoustic length scale r_s was not treated as free parameter.

BAO measurements alone from galaxy surveys provide the constraints on the Ω_{m0} but not on the Hubble parameter H_0 . Therefore, combining the GW-BAO measurements and galaxy-BAO measurements shall provide the combined constraints on parameters Ω_{m0} and H_0 . We expect that current and future spectroscopic surveys such as SDSS (Almeida et al. 2023), Euclid (Laujeijs et al. 2011), Vera C. Rubin Observatory (LSST) (Ivezić et al. 2019) will provide more robust BAO measurements by the time 3G detectors are operational. However, in this study, we use current galaxy-BAO measurements and combine them with projected GW-BAO measurements from the simulations done for 3G GW detectors to get conservative estimates of constraining power of the combination of the data. We use the current BAO measurements for the angular scales: clustering measurements on $D_M(z)/r_s$ and $D_V(z)/r_s$ at various redshifts as compiled in the data from SDSS, SDSS-II, BOSS, and eBOSS (Alam et al. 2021). We call the constraints from Galaxy-BAO likelihood functions to be SDSS-BAO+CMB constraints. We combined data sets by multiplying the GW-BAO+CMB likelihood and SDSS-BAO+CMB likelihood.

In figures 4, 5, and 6, we show the combined constraints (GW-BAO+SDSS-BAO+CMB) on the parameters of the models Λ CDM, w CDM, and w_0w_a CDM respectively. In table 3, we collect results from the constraints obtained on various cosmological parameters with different combinations of data sets. We observe that i) GW-BAO+CMB data alone can constrain the Hubble parameter but not other cosmological parameters. ii) Spectroscopic BAO measurements alone can not constrain the Hubble parameter but they can constrain other cosmological parameters such as density parameter Ω_{m0} , and dark energy parameters. iii) These two data sets are complementary to each other and hence combining them will allow us to constrain the cosmological models from BAO measurements alone, and iv) the constraints on H_0 are relatively weaker if we allow the parameter r_s to vary.

Although, as an example, we show here only a few selected parametrized DE models, this could also be applied to study other DE models, such as canonical and non-canonical scalar field models (Wetterich 1988;

Table 3. The constraints obtained on cosmological parameters corresponding to the models listed in table 1. For each parameter, 68% (90%) confidence intervals are reported. The GW-BAO constraints come from the BAO observation from the simulated GW BNS mergers for 3G detectors. For GW-BAO+CMB constraints, we calculate the comoving BAO scale r_s from sampling cosmological parameters of the model. EM counterpart constraints indicate that one BNS merger event have an EM counterpart. SDSS-BAO+CMB constraints arise from the measurement of BAO features in SDSS data, and calculating the r_s value. The entries with dashed lines indicate that the particular data do not constrain the given parameter i.e. the posterior obtained on these parameters just return the prior distribution. The empty entries indicate that the parameter is calculated from other sampling parameter and cosmology model. The ranges of the Uniform prior for each parameter are shown.

Parameter	Prior Range	Model	GW-BAO +CMB	GW-BAO +EM counterpart (r_s varying)	GW-BAO +CMB +EM counterpart	SDSS-BAO	GW-BAO +SDSS-BAO +CMB	GW-BAO +SDSS-BAO +CMB +EM counterpart	GW-BAO +SDSS-BAO +CMB +EM counterpart (r_s varying)
H_0 (km s ⁻¹ Mpc ⁻¹)	$\mathcal{U}(20, 150)$	ΛCDM	59.4 ^{+18.0} _{-12.1} (59.4 ^{+33.9} _{-17.7})	72.9 ^{+28.5} _{-20.8} (72.9 ^{+49.8} _{-31.6})	63.5 ^{+20.9} _{-14.3} (63.5 ^{+37.0} _{-21.3})	–	65.9 ^{+12.8} _{-10.2} (65.9 ^{+21.4} _{-14.8})	68.8 ^{+15.8} _{-12.2} (68.8 ^{+27.6} _{-18.5})	74.3 ^{+28.5} _{-20.4} (74.3 ^{+50.2} _{-31.3})
		wCDM	59.0 ^{+17.4} _{-12.0} (59.0 ^{+32.2} _{-17.7})	73.3 ^{+28.5} _{-20.9} (73.3 ^{+51.8} _{-32.2})	63.9 ^{+19.3} _{-14.3} (63.9 ^{+35.6} _{-21.3})	–	66.9 ^{+12.6} _{-10.2} (66.9 ^{+21.7} _{-15.4})	69.5 ^{+15.7} _{-12.4} (69.5 ^{+27.9} _{-18.9})	75.8 ^{+29.0} _{-21.5} (75.8 ^{+51.1} _{-32.2})
		w_0w_a CDM	58.7 ^{+18.1} _{-11.9} (58.7 ^{+33.9} _{-17.7})	72.9 ^{+29.3} _{-20.9} (72.9 ^{+51.8} _{-31.6})	63.4 ^{+19.3} _{-13.9} (63.4 ^{+36.3} _{-20.6})	–	65.9 ^{+12.7} _{-10.2} (65.9 ^{+21.8} _{-15.3})	68.3 ^{+15.8} _{-12.0} (68.3 ^{+27.9} _{-18.3})	75.5 ^{+28.7} _{-21.7} (75.5 ^{+51.0} _{-32.5})
Ω_{m0}	$\mathcal{U}(0.05, 1)$	ΛCDM	–	–	–	0.30 ^{+0.02} _{-0.02} (0.30 ^{+0.04} _{-0.04})	0.30 ^{+0.02} _{-0.02} (0.30 ^{+0.04} _{-0.04})	0.29 ^{+0.03} _{-0.02} (0.29 ^{+0.04} _{-0.04})	0.30 ^{+0.03} _{-0.02} (0.30 ^{+0.04} _{-0.04})
		wCDM	–	–	–	0.28 ^{+0.02} _{-0.02} (0.28 ^{+0.05} _{-0.04})	0.28 ^{+0.02} _{-0.02} (0.28 ^{+0.05} _{-0.04})	0.29 ^{+0.03} _{-0.02} (0.29 ^{+0.04} _{-0.04})	0.28 ^{+0.03} _{-0.02} (0.28 ^{+0.05} _{-0.04})
		w_0w_a CDM	–	–	–	0.29 ^{+0.04} _{-0.04} (0.29 ^{+0.06} _{-0.07})	0.29 ^{+0.04} _{-0.04} (0.29 ^{+0.06} _{-0.07})	0.30 ^{+0.04} _{-0.03} (0.30 ^{+0.06} _{-0.05})	0.29 ^{+0.04} _{-0.04} (0.29 ^{+0.06} _{-0.07})
r_s (Mpc)	$\mathcal{U}(50, 250)$	ΛCDM	–	137.1 ^{+31.2} _{-30.2} (137.1 ^{+52.8} _{-46.5})	–	–	–	–	137.2 ^{+32.0} _{-29.5} (137.2 ^{+53.4} _{-45.1})
		wCDM	–	136.8 ^{+32.1} _{-29.8} (136.8 ^{+54.2} _{-47.6})	–	–	–	–	138.4 ^{+31.7} _{-29.8} (138.4 ^{+52.0} _{-45.8})
		w_0w_a CDM	–	137.3 ^{+31.3} _{-31.1} (137.3 ^{+52.3} _{-47.7})	–	–	–	–	138.0 ^{+32.1} _{-30.4} (138.0 ^{+53.0} _{-46.4})
w	$\mathcal{U}(-2, 0)$	wCDM	–	–	–	–1.25 ^{+0.34} _{-0.35} (–1.25 ^{+0.54} _{-0.56})	–1.25 ^{+0.33} _{-0.33} (–1.25 ^{+0.53} _{-0.57})	–1.23 ^{+0.33} _{-0.36} (–1.23 ^{+0.53} _{-0.56})	–1.25 ^{+0.33} _{-0.36} (–1.25 ^{+0.53} _{-0.57})
w_0	$\mathcal{U}(-2, 0)$	w_0w_a CDM	–	–	–	–1.05 ^{+0.46} _{-0.47} (–1.05 ^{+0.73} _{-0.75})	–1.05 ^{+0.47} _{-0.47} (–1.05 ^{+0.73} _{-0.76})	–1.02 ^{+0.47} _{-0.49} (–1.02 ^{+0.72} _{-0.76})	–1.06 ^{+0.47} _{-0.48} (–1.06 ^{+0.73} _{-0.74})
w_a	$\mathcal{U}(-4, 4)$	w_0w_a CDM	–	–	–	–1.31 ^{+2.05} _{-1.86} (–1.31 ^{+2.79} _{-2.42})	–1.43 ^{+2.05} _{-1.76} (–1.43 ^{+2.78} _{-2.30})	–1.45 ^{+1.95} _{-1.77} (–1.45 ^{+2.71} _{-2.30})	–1.28 ^{+2.02} _{-1.85} (–1.28 ^{+2.75} _{-2.45})

Ratra & Peebles 1988; Peebles & Ratra 1988; Turner & White 1997; Caldwell et al. 1998; Zlatev et al. 1999; Bagla et al. 2003), Galileon models (Nicolis et al. 2009; Ali et al. 2010; Gannouji & Sami 2010), and other models of cosmology based on modified gravity theories (Clifton et al. 2012).

4. SUMMARY

The future of GW cosmology looks bright as the growing catalog of GW mergers provides us an independent probe of the Universe apart from the traditional electromagnetic window. The independent probes offers us not only additional opportunities to constrain the cosmological parameters, they might also help to resolve the possible tension between various data sets such as the so called Hubble tension between current CMB data at high redshift (Aghanim et al. 2020) and SNe data from the low redshifts (Riess et al. 2019). With the current catalog of GW events, the localization volumes (from BBHs) can be used along with galaxy catalogs using cross correlation techniques to constrain the Hubble constant H_0 (Abbott et al. 2021a). In case of BNS events which have electromagnetic counterparts (e.g. GW170817), more stringent constraints on H_0 can be put because of the precise redshift information (Abbott et al. 2017d). In the future, we expect these constraints to become stringent with more GW merger observations

as we expect to detect EM counterparts for a small fraction of events (such as nearby BNS/NSBH mergers).

The third generation of GW detectors such as ET and CE are expected to be order of magnitude more sensitive than current generation detectors, and will be able to probe lower frequencies upto few Hz (Reitze et al. 2019; Sathyaprakash et al. 2012). It will enable them to detect thousands of GW mergers with precise enough localization to probe the large scale structures of the Universe using their localization volumes solely from the GW merger observations (Vijaykumar et al. 2020). We should be able to probe the LSS features such as galaxy bias, and BAO peak by measuring the 2PCF from the localization volumes (Kumar et al. 2022; Vijaykumar et al. 2020). In this study we show that, with 3G detector network, by tracing the angular BAO scale from GW mergers $\theta_{BAO}(D_L)$ at various luminosity distance bins, we can put constraints on the cosmological parameters such as the Hubble constant H_0 (for ΛCDM model) with 90% credible intervals $H_0 = 59.4^{+33.9}_{-17.7}$ km s⁻¹ Mpc⁻¹. We show that the constraints on the cosmological parameters from GW-BAO data are complementary to the constraints obtained from galaxy-BAO measurements. Therefore, when these data sets are combined, it will enable us to constrain the parameters of various dark energy models. In this study, as a proof of concept, we combine the expected BAO constraints from GW mergers from the 3G detector network along with the BAO measurements from current spectroscopic surveys,

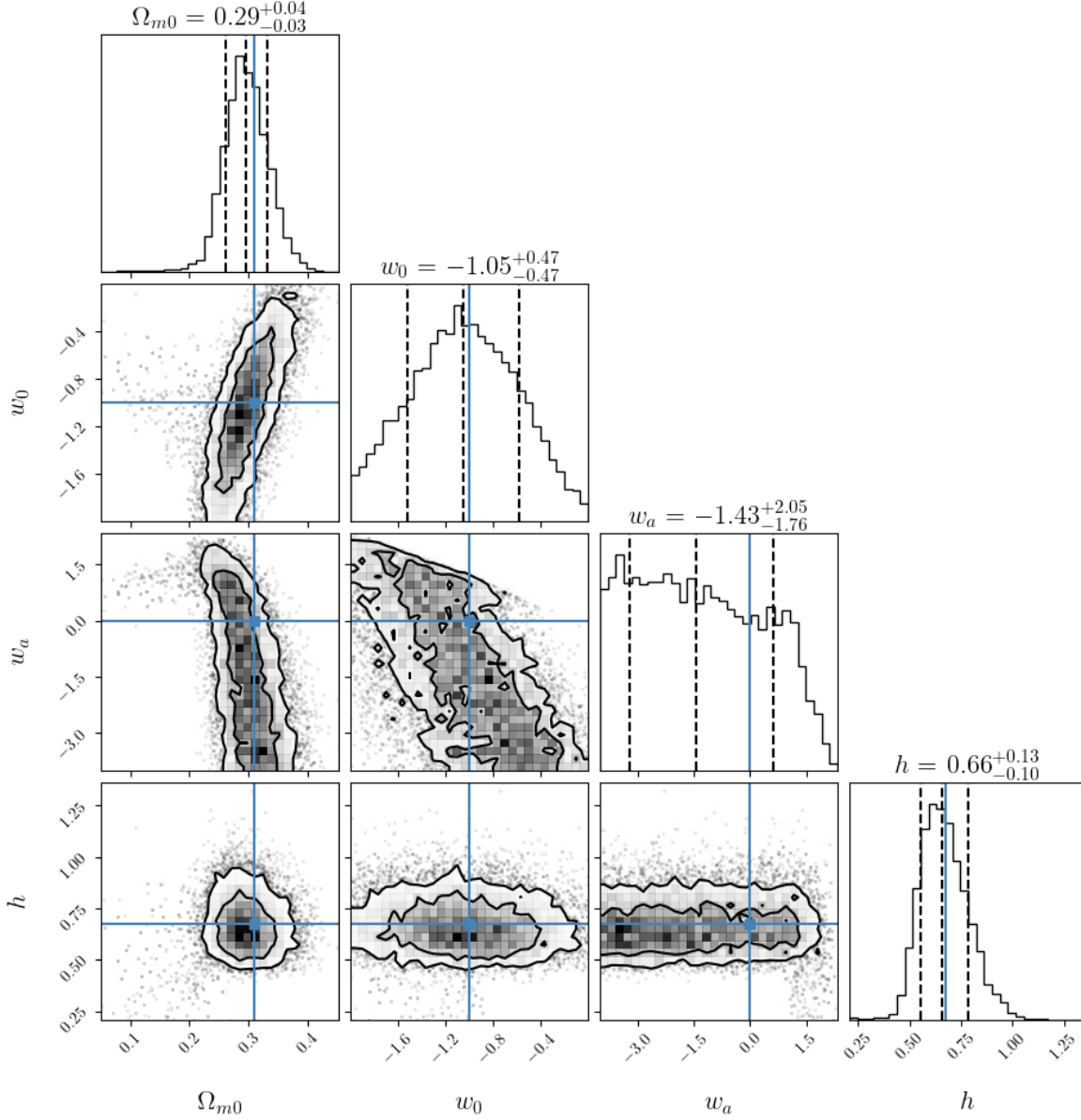


Figure 6. The combined constraints (GW-BAO+SDSS-BAO+CMB) on the w_0w_a CDM model with BAO measurements from GW localization volumes (from simulations) and CMB/BAO constraints from the galaxy surveys. For the marginalized 1D posteriors, we show 68% bounds with the median value. For 2D contours, we show 60% and 90% regions. The injected values are shown by blue lines corresponding to the Λ CDM model with parameters consistent with the *Planck2018* results (Aghanim et al. 2020).

though we expect the future spectroscopic surveys to be outperforming the current generation of galaxy surveys. Therefore, the results presented in this study are the conservative estimates. We would also like to emphasize that, this is not a unique method to put constraints on cosmological parameters as more stringent constraints can be provided by various combination of data from other cosmological surveys e.g. CMB, type Ia supernovae, etc. However, it will still provide an independent probe of cosmology which can be combined

with the available data from future galaxy surveys to put tighter constraints and in the best case, help in resolving the tension between the competing data sets, if any. This study adds to the science case of 3G detectors and build on the previous studies on probing LSS with 3G detectors network (Kumar et al. 2022; Vijaykumar et al. 2020).

ACKNOWLEDGMENTS

We acknowledge the Max Planck Gesellschaft. We thank the computing team from AEI Hannover for their significant technical support. SK thanks Xisco Jiménez Forteza and Pierre Mourier for going through the manuscript and providing useful comments. SK also thanks Aditya Vijaykumar and Anjan Sen for useful discussions. SK thanks the anonymous referee for critical inputs and improving the manuscript. ATLAS cluster at AEI Hannover was used to perform all the computational work done in this study.

REFERENCES

- Aasi, J., et al. 2015, *Class. Quant. Grav.*, 32, 074001, doi: [10.1088/0264-9381/32/7/074001](https://doi.org/10.1088/0264-9381/32/7/074001)
- Abbott, B. P., et al. 2016, *Phys. Rev. D*, 93, 122003, doi: [10.1103/PhysRevD.93.122003](https://doi.org/10.1103/PhysRevD.93.122003)
- Abbott, B. P., Abbott, R., Abbott, T. D., et al. 2017a, *Phys. Rev. Lett.*, 119, 161101, doi: [10.1103/PhysRevLett.119.161101](https://doi.org/10.1103/PhysRevLett.119.161101)
- Abbott, B. P., et al. 2017b, *Astrophys. J. Lett.*, 848, L12, doi: [10.3847/2041-8213/aa91c9](https://doi.org/10.3847/2041-8213/aa91c9)
- . 2017c, *Astrophys. J. Lett.*, 848, L13, doi: [10.3847/2041-8213/aa920c](https://doi.org/10.3847/2041-8213/aa920c)
- . 2017d, *Nature*, 551, 85, doi: [10.1038/nature24471](https://doi.org/10.1038/nature24471)
- . 2018a, *Phys. Rev. Lett.*, 121, 161101, doi: [10.1103/PhysRevLett.121.161101](https://doi.org/10.1103/PhysRevLett.121.161101)
- . 2018b, *Living Rev. Rel.*, 21, 3, doi: [10.1007/s41114-020-00026-9](https://doi.org/10.1007/s41114-020-00026-9)
- Abbott, B. P., Abbott, R., Abbott, T. D., et al. 2018, *Living Reviews in Relativity*, 21, 3, doi: [10.1007/s41114-018-0012-9](https://doi.org/10.1007/s41114-018-0012-9)
- Abbott, B. P., et al. 2021a, *Astrophys. J.*, 909, 218, doi: [10.3847/1538-4357/abdc7](https://doi.org/10.3847/1538-4357/abdc7)
- Abbott, R., et al. 2021b. <https://arxiv.org/abs/2111.03606>
- . 2021c. <https://arxiv.org/abs/2111.03634>
- . 2021d. <https://arxiv.org/abs/2112.06861>
- . 2021e. <https://arxiv.org/abs/2111.03604>
- Abbott, R., Abbott, T. D., Abraham, S., et al. 2021, *ApJL*, 913, L7, doi: [10.3847/2041-8213/abe949](https://doi.org/10.3847/2041-8213/abe949)
- Acernese, F., et al. 2015, *Class. Quant. Grav.*, 32, 024001, doi: [10.1088/0264-9381/32/2/024001](https://doi.org/10.1088/0264-9381/32/2/024001)
- Aghanim, N., et al. 2020, *Astron. Astrophys.*, 641, A6, doi: [10.1051/0004-6361/201833910](https://doi.org/10.1051/0004-6361/201833910)
- Agrawal, A., Makiya, R., Chiang, C.-T., et al. 2017, *Journal of Cosmology and Astroparticle Physics*, 2017, 003003, doi: [10.1088/1475-7516/2017/10/003](https://doi.org/10.1088/1475-7516/2017/10/003)
- Akutsu, T., et al. 2021, *PTEP*, 2021, 05A101, doi: [10.1093/ptep/ptaa125](https://doi.org/10.1093/ptep/ptaa125)
- Alam, S., et al. 2021, *Phys. Rev. D*, 103, 083533, doi: [10.1103/PhysRevD.103.083533](https://doi.org/10.1103/PhysRevD.103.083533)
- Ali, A., Gannouji, R., & Sami, M. 2010, *Phys. Rev. D*, 82, 103015, doi: [10.1103/PhysRevD.82.103015](https://doi.org/10.1103/PhysRevD.82.103015)
- Almeida, A., Anderson, S. F., Argudo-Fernández, M., et al. 2023, *arXiv e-prints*, arXiv:2301.07688, doi: [10.48550/arXiv.2301.07688](https://doi.org/10.48550/arXiv.2301.07688)
- Bagla, J. S., Jassal, H. K., & Padmanabhan, T. 2003, *Phys. Rev. D*, 67, 063504, doi: [10.1103/PhysRevD.67.063504](https://doi.org/10.1103/PhysRevD.67.063504)
- Bassett, B. A., & Hlozek, R. 2009. <https://arxiv.org/abs/0910.5224>
- Baumann, D. 2011, in *Theoretical Advanced Study Institute in Elementary Particle Physics: Physics of the Large and the Small*, 523–686, doi: [10.1142/9789814327183_0010](https://doi.org/10.1142/9789814327183_0010)
- Borhanian, S., & Sathyaprakash, B. S. 2022. <https://arxiv.org/abs/2202.11048>
- Caldwell, R. R., Dave, R., & Steinhardt, P. J. 1998, *Phys. Rev. Lett.*, 80, 1582, doi: [10.1103/PhysRevLett.80.1582](https://doi.org/10.1103/PhysRevLett.80.1582)
- Capano, C. D., Tews, I., Brown, S. M., et al. 2020, *Nature Astron.*, 4, 625, doi: [10.1038/s41550-020-1014-6](https://doi.org/10.1038/s41550-020-1014-6)
- Chen, H.-Y., Cowperthwaite, P. S., Metzger, B. D., & Berger, E. 2021, *Astrophys. J. Lett.*, 908, L4, doi: [10.3847/2041-8213/abdab0](https://doi.org/10.3847/2041-8213/abdab0)
- Chevallier, M., & Polarski, D. 2001, *Int. J. Mod. Phys. D*, 10, 213, doi: [10.1142/S0218271801000822](https://doi.org/10.1142/S0218271801000822)
- Clifton, T., Ferreira, P. G., Padilla, A., & Skordis, C. 2012, *Physics Reports*, 513, 1, doi: [10.1016/j.physrep.2012.01.001](https://doi.org/10.1016/j.physrep.2012.01.001)
- Coles, P., & Erdogdu, P. 2007, *JCAP*, 10, 007, doi: [10.1088/1475-7516/2007/10/007](https://doi.org/10.1088/1475-7516/2007/10/007)
- Dalal, N., Holz, D. E., Hughes, S. A., & Jain, B. 2006, *Phys. Rev. D*, 74, 063006, doi: [10.1103/PhysRevD.74.063006](https://doi.org/10.1103/PhysRevD.74.063006)

- Eisenstein, D. J., & Hu, W. 1998, *Astrophys. J.*, 496, 605, doi: [10.1086/305424](https://doi.org/10.1086/305424)
- Eisenstein, D. J., et al. 2005, *Astrophys. J.*, 633, 560, doi: [10.1086/466512](https://doi.org/10.1086/466512)
- Evans, M., Adhikari, R. X., Afle, C., et al. 2021, arXiv e-prints, arXiv:2109.09882. <https://arxiv.org/abs/2109.09882>
- Fairhurst, S. 2014, *J. Phys. Conf. Ser.*, 484, 012007, doi: [10.1088/1742-6596/484/1/012007](https://doi.org/10.1088/1742-6596/484/1/012007)
- Gannouji, R., & Sami, M. 2010, *Phys. Rev. D*, 82, 024011, doi: [10.1103/PhysRevD.82.024011](https://doi.org/10.1103/PhysRevD.82.024011)
- Giostrì, R., dos Santos, M. V., Waga, I., et al. 2012, *JCAP*, 03, 027, doi: [10.1088/1475-7516/2012/03/027](https://doi.org/10.1088/1475-7516/2012/03/027)
- Guth, A. H. 1981, *Phys. Rev. D*, 23, 347, doi: [10.1103/PhysRevD.23.347](https://doi.org/10.1103/PhysRevD.23.347)
- Holz, D. E., & Hughes, S. A. 2005, *Astrophys. J.*, 629, 15, doi: [10.1086/431341](https://doi.org/10.1086/431341)
- Hu, W., & Dodelson, S. 2002, *Ann. Rev. Astron. Astrophys.*, 40, 171, doi: [10.1146/annurev.astro.40.060401.093926](https://doi.org/10.1146/annurev.astro.40.060401.093926)
- Ivezić, v., et al. 2019, *Astrophys. J.*, 873, 111, doi: [10.3847/1538-4357/ab042c](https://doi.org/10.3847/1538-4357/ab042c)
- Kumar, S., Vijaykumar, A., & Nitz, A. H. 2022, *Astrophys. J.*, 930, 113, doi: [10.3847/1538-4357/ac5e34](https://doi.org/10.3847/1538-4357/ac5e34)
- Landy, S. D., & Szalay, A. S. 1993, *Astrophys. J.*, 412, 64, doi: [10.1086/172900](https://doi.org/10.1086/172900)
- Laureijs, R., Amiaux, J., Arduini, S., et al. 2011, *Euclid Definition Study Report*, arXiv, doi: [10.48550/ARXIV.1110.3193](https://doi.org/10.48550/ARXIV.1110.3193)
- Linde, A. D. 1982, *Phys. Lett. B*, 108, 389, doi: [10.1016/0370-2693\(82\)91219-9](https://doi.org/10.1016/0370-2693(82)91219-9)
- Mastrogiovanni, S., Leyde, K., Karathanasis, C., et al. 2021, *Phys. Rev. D*, 104, 062009, doi: [10.1103/PhysRevD.104.062009](https://doi.org/10.1103/PhysRevD.104.062009)
- Mills, C., Tiwari, V., & Fairhurst, S. 2018, *Phys. Rev.*, D97, 104064, doi: [10.1103/PhysRevD.97.104064](https://doi.org/10.1103/PhysRevD.97.104064)
- Mukherjee, S., Wandelt, B. D., Nissanke, S. M., & Silvestri, A. 2021, *Phys. Rev. D*, 103, 043520, doi: [10.1103/PhysRevD.103.043520](https://doi.org/10.1103/PhysRevD.103.043520)
- Nicolis, A., Rattazzi, R., & Trincherini, E. 2009, *Phys. Rev. D*, 79, 064036, doi: [10.1103/PhysRevD.79.064036](https://doi.org/10.1103/PhysRevD.79.064036)
- Nissanke, S., Holz, D. E., Dalal, N., et al. 2013. <https://arxiv.org/abs/1307.2638>
- Nitz, A. H., & Dal Canton, T. 2021, *The Astrophysical Journal Letters*, 917, L27, doi: [10.3847/2041-8213/ac1a75](https://doi.org/10.3847/2041-8213/ac1a75)
- Nitz, A. H., Kumar, S., Wang, Y.-F., et al. 2021, 4-OGC: Catalog of gravitational waves from compact-binary mergers. <https://arxiv.org/abs/2112.06878>
- Peebles, P. J. E. 1980, *The large-scale structure of the universe*
- Peebles, P. J. E., & Ratra, B. 1988, *Astrophys. J. Lett.*, 325, L17, doi: [10.1086/185100](https://doi.org/10.1086/185100)
- Petrov, P., Singer, L. P., Coughlin, M. W., et al. 2022, *ApJ*, 924, 54, doi: [10.3847/1538-4357/ac366d](https://doi.org/10.3847/1538-4357/ac366d)
- Punturo, M., Abernathy, M., Acernese, F., et al. 2010, *Classical and Quantum Gravity*, 27, 194002, doi: [10.1088/0264-9381/27/19/194002](https://doi.org/10.1088/0264-9381/27/19/194002)
- Ratra, B., & Peebles, P. J. E. 1988, *Phys. Rev. D*, 37, 3406, doi: [10.1103/PhysRevD.37.3406](https://doi.org/10.1103/PhysRevD.37.3406)
- Reitze, D., et al. 2019, *Bull. Am. Astron. Soc.*, 51, 035. <https://arxiv.org/abs/1907.04833>
- Riess, A. G., Casertano, S., Yuan, W., Macri, L. M., & Scolnic, D. 2019, *Astrophys. J.*, 876, 85, doi: [10.3847/1538-4357/ab1422](https://doi.org/10.3847/1538-4357/ab1422)
- Riess, A. G., & et al. 1998, *The Astronomical Journal*, 116, 1009, doi: [10.1086/300499](https://doi.org/10.1086/300499)
- Riess, A. G., et al. 2021. <https://arxiv.org/abs/2112.04510>
- Saleem, M., et al. 2022, *Class. Quant. Grav.*, 39, 025004, doi: [10.1088/1361-6382/ac3b99](https://doi.org/10.1088/1361-6382/ac3b99)
- Sathyaprakash, B., et al. 2012, *Class. Quant. Grav.*, 29, 124013, doi: [10.1088/010264-9381/29/12/124013](https://doi.org/10.1088/010264-9381/29/12/124013)
- Speagle, J. S. 2020, *Monthly Notices of the Royal Astronomical Society*, 493, 3132, doi: [10.1093/mnras/staa278](https://doi.org/10.1093/mnras/staa278)
- Turner, M. S., & White, M. J. 1997, *Phys. Rev. D*, 56, R4439, doi: [10.1103/PhysRevD.56.R4439](https://doi.org/10.1103/PhysRevD.56.R4439)
- Vijaykumar, A., Saketh, M. V. S., Kumar, S., Ajith, P., & Choudhury, T. R. 2020. <https://arxiv.org/abs/2005.01111>
- Weinberg, D. H. 2013, *Physics Reports*, 530, 87, doi: [10.1016/j.physrep.2013.05.001](https://doi.org/10.1016/j.physrep.2013.05.001)
- Weinberg, D. H., Mortonson, M. J., Eisenstein, D. J., et al. 2013, *Phys. Rept.*, 530, 87, doi: [10.1016/j.physrep.2013.05.001](https://doi.org/10.1016/j.physrep.2013.05.001)
- Wetterich, C. 1988, *Nucl. Phys. B*, 302, 668, doi: [10.1016/0550-3213\(88\)90193-9](https://doi.org/10.1016/0550-3213(88)90193-9)
- Zlatev, I., Wang, L.-M., & Steinhardt, P. J. 1999, *Phys. Rev. Lett.*, 82, 896, doi: [10.1103/PhysRevLett.82.896](https://doi.org/10.1103/PhysRevLett.82.896)